# Dynamic Rheological Study of Paraffin Wax and Its Organoclay Nanocomposites

**Jinfeng Wang, Mark D. Calhoun, Steven J. Severtson**

*Department of Bioproducts and Biosystems Engineering, University of Minnesota, 2004 Folwell Avenue, St. Paul, Minnesota 55108*

Received 20 September 2007; accepted 14 November 2007
DOI 10.1002/app.27768
Published online 20 February 2008 in Wiley InterScience (www.interscience.wiley.com).

**ABSTRACT:** Dynamic rheological data for paraffin wax and its organoclay nanocomposites are reported. Dynamic mechanical analysis of paraffin wax for temperatures ranging from −40 to 55°C showed a decrease of several orders of magnitude in the dynamic moduli and a significant shift toward viscous behavior, which resulted from the occurrence of two solid–solid phase transitions. In both the crystalline and mesophase regions, the dispersion of organoclay platelets in paraffin wax via ultrasonication increased the storage modulus, whereas the effect on the loss modulus was temperature-dependent. The melt rheology data of the wax–clay nanocomposites at 70°C showed that the complex viscosities increased monotonically with clay addition and demonstrated shear-thinning behavior for frequencies between 0.1 and 100 rad/s. The complex viscosity versus angular frequency data were well fit by a power-law function for which the shear-thinning exponent provides a gauge for the extent of clay exfoliation. The nanocomposites exhibited low-frequency solid behavior, which indicated good exfoliation of the organoclay in the wax matrix. © 2008 Wiley Periodicals, Inc. J Appl Polym Sci 108: 2564–2570, 2008

**Key words:** nanocomposites; oligomers; organoclay; rheology

## INTRODUCTION

Paraffin (macrocrystalline) wax is a mixture of hydrocarbons consisting mainly of normal alkanes with carbon numbers that range from about 18 to 45. As a low-cost petroleum byproduct, wax is attractive as a raw material. However, it is quite weak and brittle and, thus, is ill-suited for applications requiring structural stability. In previous work,[1,2] we reported the tensile properties and structures of nanocomposites produced through the intercalation and exfoliation of organically modified clay in a commercial paraffin wax. This was part of a research effort to develop high-performance, low-cost barrier coatings. These nanocomposites were shown to possess significantly greater stiffness and yield strength relative to the pure wax for low organoclay loadings. More impressive was the observation that their ductility, as gauged by elongation at break, increased nearly four-fold at 25°C. We also reported that enhancements of the tensile properties diminished as the wax-based materials thermally neared the lowest temperature solid–solid phase transition for the paraffin wax at about 30°C, upon which the wax entered into its mesophase region. Accurate tensile measurements above these temperatures were not possible due to the increased fluidity of the wax matrix.

In this study, we investigated the viscoelastic properties of paraffin wax and its organoclay nanocomposites over a broad temperature range that included its low-temperature crystalline state, mesophase region, and melt. Because of its low molecular weight and unusual phase behavior, the rheological properties of paraffin wax are difficult to characterize, and there are few published studies on this topic.[3–6] We believe that this is the first study on the dynamic rheological properties of paraffin wax and its composites over a broad temperature range and the first such study of an organoclay nanocomposite generated with an oligomeric matrix. The results indicate that strong interactions between the organoclay and wax matrices were retained in the mesophase region. It is also demonstrated that the melt rheology curve may provide a method for gauging the degree to which the organoclay is exfoliated in generated composites.

## EXPERIMENTAL

### Materials

Paraffin wax (IGI 1230A) with a differential scanning calorimetry (DSC) melting point of 53°C was supplied by the International Group, Inc. (Toronto, Canada). Cloisite 20A, a natural montmorillonite modi-

*Correspondence to:* S. J. Severtson (sever018@umn.edu).
Contract grant sponsor: U.S. Department of Energy; contract grant number: DE-FC36-04GO14309.

fied with a quaternary ammonium salt, was obtained from Southern Clay Products, Inc. (Gonzales, TX). Wax–clay nanocomposites with clay concentrations of 0.5, 1, 2, 3, and 5 wt % were prepared with an ultrasonic processor. The procedure was described in a previous article.[1] A wax–clay composite with 3 wt % clay was also prepared by mixing with a magnetic stirrer bar at a temperature above the melting point of the wax.

### Characterization of the materials

The phase transitions of paraffin wax were studied with a TA Instruments (New Castle, DE) Q1000 differential scanning calorimeter. Thermograms were obtained under a helium atmosphere over a temperature range of 15–65°C with heating/cooling rates of 10°C/min. The first heating, first cooling, and second heating cycles were collected. X-ray diffraction (XRD) was carried out on a Scintag (Cupertino, CA) XDS 2000 θ/θ goniometer with a 2.2-kW sealed copper X-ray source and a solid–solid detector. Crushed wax was added to a copper sample holder (25 mm × 25 mm × 1 mm) to fill the inscribed circle (diameter = 10 mm, depth = 0.5 mm). The sample holder with wax in it was then heated on a hot plate to allow the wax to melt. Excess molten wax was removed by absorbtion with tissue paper. After they were cooled to room temperature, wax samples were scanned with a 2θ range of 1.5–30°. The temperature of the samples was raised at a rate of 0.5°C/min to obtain scans for temperatures of 25, 30, 32, 33, 35, 37, and 39°C.

Three geometries and two rheometers were used to collect rheological data for the paraffin wax and its organoclay nanocomposites. For solid samples, dynamic shear measurements were conducted on an ARES rheometer with air-bearing motor and a 2K force rebalance transducer (TA Instruments, New Castle, DE). Below 36°C, where the wax was in its low-temperature crystalline state, rectangular specimens (ca. $2\frac{1}{4}$ in. long, $\frac{1}{2}$ in. wide, and $\frac{1}{16}$ in. thick) were measured with torsion rectangular geometry. Throughout the mesophase region for the wax, from about 36 to 55°C, parallel plate (8 mm diameter) geometry was used. A strain sweep was performed for each sample at 1 rad/s to obtain the linear viscoelastic region. Temperature ramps were conducted at a ramping rate of 3°C/min and an angular frequency (ω) of 1.0 rad/s. Strain frequency sweeps were collected from 100 to 0.1 rad/s at −50 and 40°C. Dynamic shear measurements were also conducted on the molten wax–clay nanocomposites with a TA Instruments AR-G2 instrument with parallel plates with a diameter of 40 mm. Strain (nanocomposites) sweeps were conducted on each sample to identify the linear viscoelastic region, and dynamic frequency sweeps were conducted at 70°C from 100 to 0.1 rad/s.

## RESULTS AND DISCUSSION

### Phase behavior of paraffin wax and its nanocomposites

Paraffin waxes demonstrate complex phase behavior. Between fully ordered crystalline states and isotropic liquid phases, waxes possess several layered plastic crystalline mesophases, in which molecules retain positional order on gaining a rotational degree of freedom about their long axes. These states are common for normal alkane mixtures including paraffin waxes and are often referred to as *rotator phases* and *premelting states* given the increased rotational freedom and thermal location just before the melting points, respectively. The structures of rotator phases in individual and binary mixtures of normal alkanes have been examined extensively with thermal analysis and X-ray scattering, which have identified five distinct rotator phases involving spacing and tilt modifications to the low-temperature crystal structure.[7–11] In contrast, the rotator phases of real wax systems have been studied little primarily because of their complexity in composition.[12–16]

Figure 1 shows the DSC scan of the commercial paraffin wax used throughout this study. The scans shown are the cooling and second heating cycles. For the heating cycle, the lower temperature transition that began at about 22.9°C, with a peak at approximately 33.5°C, corresponded to the premelting solid–solid transition. The higher temperature transition, with a peak at 53.2°C, was the melting transition. The cooling cycle revealed two solid–solid transitions with peak temperatures of 29.5 and 32.7°C. The phase transitions of the paraffin wax were further examined with XRD. Figure 2 shows the overlay of XRD scans for the paraffin wax obtained at a series of different temperatures. At

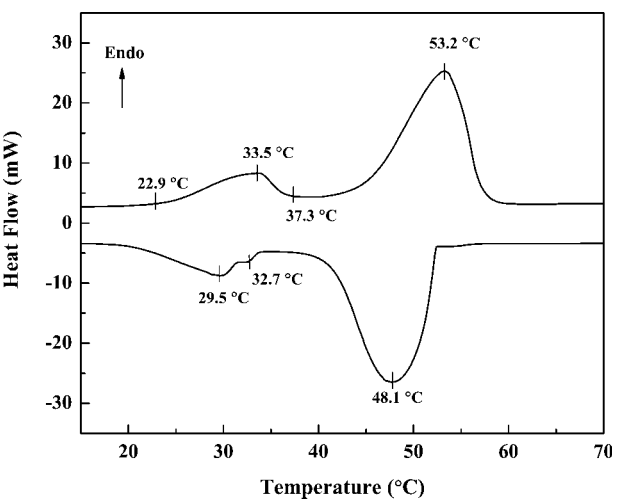


**Figure 1** DSC scans of the paraffin wax: second heating (top) and cooling (bottom).

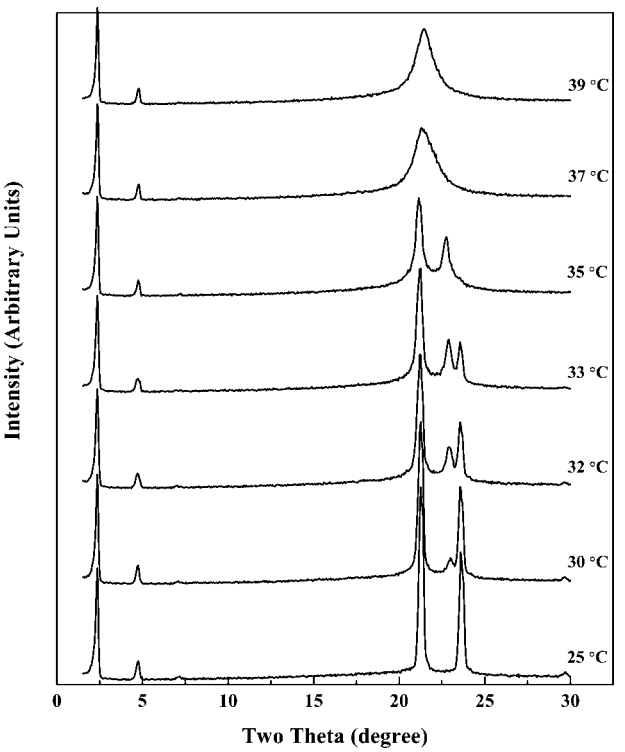


**Figure 2** XRD scans of the paraffin wax at various temperatures.

25°C, the paraffin wax possessed an orthorhombic phase. When the temperature was increased to 30°C, a high-temperature orthorhombic rotator phase appeared, which coexists with the low-temperature orthorhombic phase. With increasing temperature, there was greater conversion from the low-temperature orthorhombic phase to the high-temperature orthorhombic rotator phase. Further heating resulted in greater distortion in the basal plane until, at 37°C, a hexagonal rotator phase was reached before the melting transition. These observations are consistent with those reported by Craig and coworkers[13,14] in two recent articles, which explained the existence of the low- and high-temperature orthorhombic phases as due to preordering among the crystallizing normal alkanes. They proposed that *n*-alkanes of similar chain lengths crystallize as pockets of like-sized molecules clustering within homogeneous wax crystallites. As the temperature reaches the first rotator phase transition, molecular heterogeneous regions are induced into the rotator state, whereas the pockets of like-sized molecules are more stable and will remain in the low-temperature orthorhombic state and enter the orthorhombic rotator phase only after higher temperatures are reached.

As demonstrated in a subsequent section of this article, movement of the paraffin wax into its rotator phases substantially changed its mechanical properties. Changes in the dynamic mechanical properties in the crystalline and mesophase regions, the rheological properties in the melt, and the influence of clay on these properties are examined later.

## Dynamic mechanical analysis of the paraffin wax and its nanocomposites

Dynamic mechanical analysis was used to study the paraffin wax in both the low-temperature crystalline state with rectangular torsion bars and the rotator phase region with 8-mm parallel plates. The different geometries were used to optimize the accuracy of the measurements. A superimposed temperature sweep at 1 rad/s from −40 to 55°C for the pure paraffin wax is shown in Figure 3(a). In the plot, three regions are noted: the low-temperature crystalline

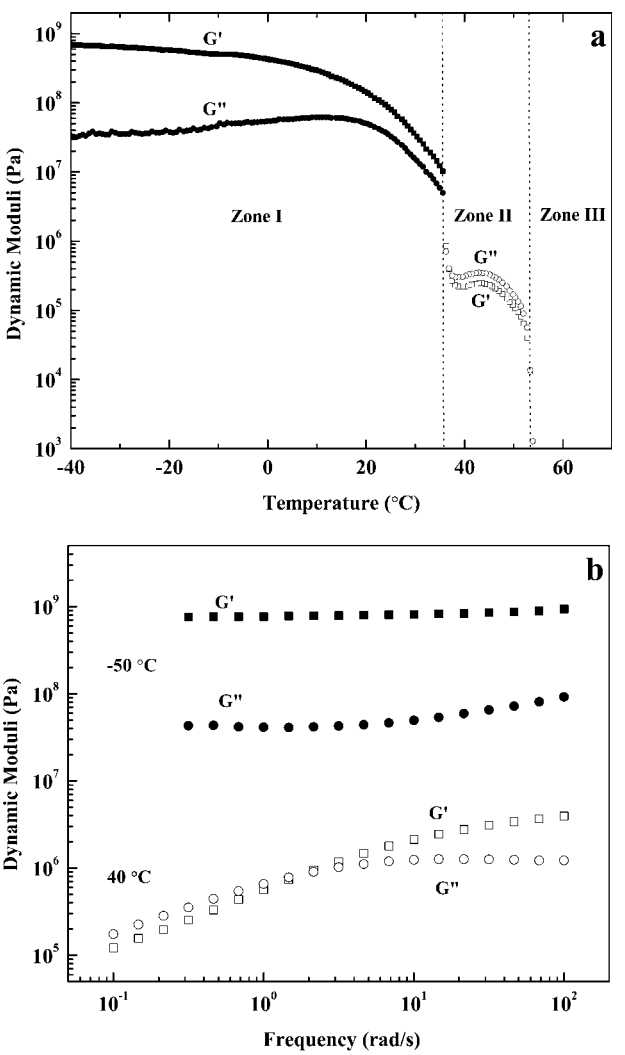


**Figure 3** (a) Temperature dependence of $G'$ and $G''$ for a commercial paraffin wax measured at a frequency of 1 rad/s. Data collected with rectangular torsion bars are indicated by solid points, whereas those obtained with 8-mm parallel plates are indicated by open points. (b) Frequency dependence of the dynamic moduli for pure paraffin wax measured at temperatures of −50 and 40°C.

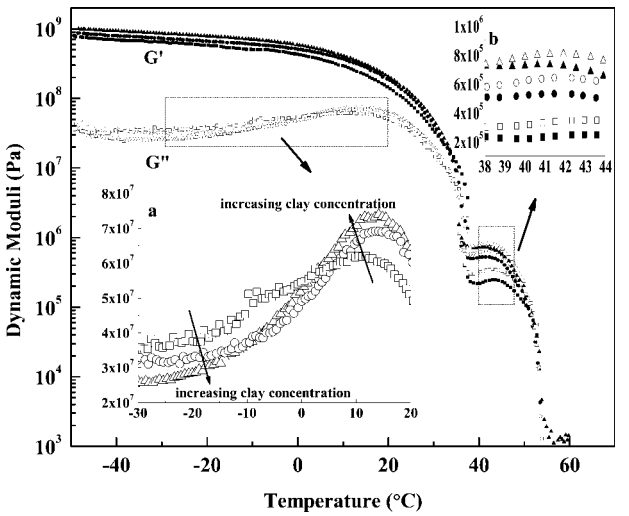


**Figure 4** Temperature dependence of $G'$ (solid symbols) and $G''$ (open symbols) collected at a frequency of 1 rad/s for (■,□) pure paraffin wax and wax nanocomposites with organoclay concentrations of (●,○) 1 and (▲,△) 3 wt %.

region (zone I); the mesophase region (zone II), which contains the rotator phases; and the isotropic liquid or melt region (zone III). As expected, on transitioning into the mesophase region, the dynamic moduli dropped sharply. The storage modulus ($G'$) decreased from $7 \times 10^8$ Pa at −40°C to below $10^6$ Pa at 40°C, and the loss modulus ($G''$) decreased from $3 \times 10^7$ to $2 \times 10^5$ Pa over the same temperature span. When the temperature was further increased to about 50°C, another sharp drop in both moduli was observed due to the onset of melting.

In addition to the sharp decrease in both $G''$ and $G'$ as paraffin wax entered the rotator phase region, there was a change in the relative magnitude of these quantities, which indicated an increase in the viscoelastic behavior. In the crystalline region (zone I), $G'$ was significantly larger than $G''$, which showed predominantly elastic behavior. On entrance to the mesophase region (zone II), $G''$ was similar but slightly larger than $G'$, which indicated a significant increase in the viscous behavior of the wax. The change in the viscoelasticity from the crystalline to the rotator phase could also been seen from the frequency sweeps [see Fig. 3(b)] of the paraffin wax obtained at −50°C (crystalline phase) and 40°C (rotator phase). At −50°C, $G'$ values were predominant over $G''$ values over the entire frequency range measured. At 40°C, the wax was solidlike at high frequencies and liquidlike at low frequencies, with a crossover occurring ($G' = G''$) at about 2 rad/s.

Figure 4 compares the dynamic moduli as a function of temperature collected at 1 rad/s for the paraffin wax and its nanocomposites with highly exfoliated organoclay concentrations of 1 and 3 wt %. The addition of clay increased $G'$ for all of the temperatures tested. For $G''$, the influence of clay was temperature-dependent. At sufficiently low temperatures (<−10°C), increasing clay concentrations reduced $G''$, but for temperatures near the mesophase transition and throughout the premelting region, clay raised $G''$. Figure 4(a) enlarges the $G''$ plot for temperatures ranging from −30 to 20°C. In this isolated region, the change in the dependence of the $G''$ values on clay content with temperature could be clearly seen. A narrowing of the phase transition peak with the addition of clay was also observed. Inset b demonstrates that the exfoliated clay had a significant impact on $G'$ and $G''$ within the mesophase region.

## Melt rheology of the clay nanocomposites

Figure 5 shows the dynamic strain sweeps for the wax nanocomposites at three different clay loadings and at a fixed temperature of 70°C, which was approximately 20°C above the melting point of the wax. Because of instrument limitation, the data on pure wax could not be reliably obtained. Large linear viscoelastic regions were observed for the nanocomposites in which $G'$ was independent of the strain. There was a reduction in the linear region for the 5 wt % clay concentration nanocomposite. Strain amplitudes of 1% were used to collect frequency sweeps for all of the nanocomposite samples. Figure 6 shows logarithmic plots of the complex viscosity ($\eta^*$) versus $\omega$ at 70°C. The $\eta^*$ values of the nanocomposites increased monotonically with organoclay loading. All of the samples demonstrated shear-thinning behavior at low frequencies. The nanocomposite

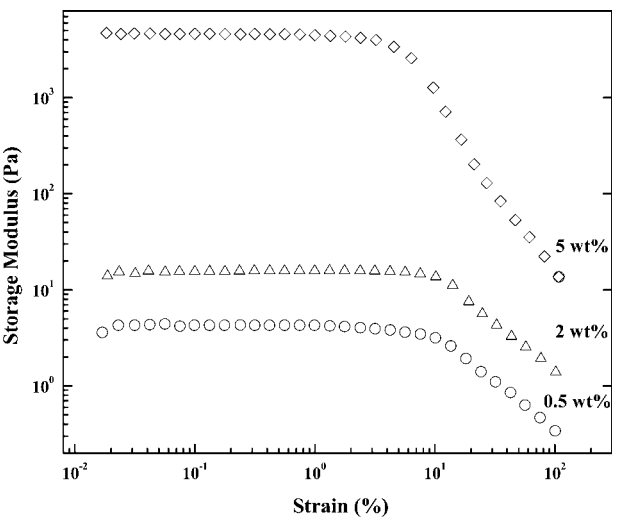


**Figure 5** Dynamic strain sweeps for wax nanocomposites containing various concentrations of organoclay. The data were collected at a temperature of 70°C and at a frequency of 1 rad/s.

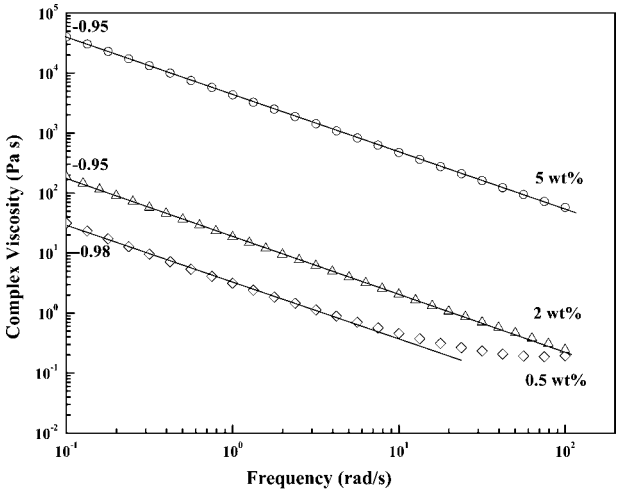


**Figure 6** Frequency dependence of η* for wax nanocomposites with various organoclay concentrations.

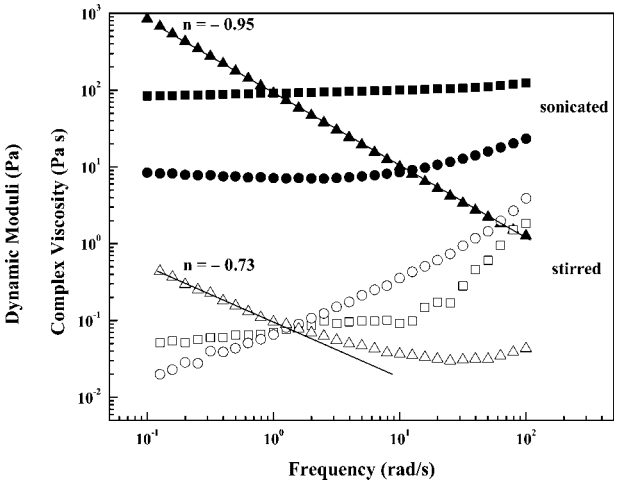


**Figure 7** Frequency dependence of (■,□) $G'$, (●,○) $G''$, and (▲,△) η* for wax nanocomposites containing 3 wt % organoclay prepared via sonication (solid symbols) and stirring (open symbols).

with 0.5 wt % clay showed a plateau region at high frequencies where the clay platelets were unable to follow the shear-induced disturbance, and the dynamics were then controlled by the liquid wax itself.[18]

The shear-thinning region was fit well by an empirical power-law expression of the following form:

$$\eta^* = A\omega^n \tag{1}$$

where $A$ and $n$ are fitting constants. Exponent $n$, extracted from linear fits of the low-frequency data, is listed next to the curves in Figure 6. This term is often referred to as the *shear-thinning exponent.* Values for the wax nanocomposites with several different organoclay concentrations were all close to −1. Wagener et al.[17] reported that the shear-thinning exponent can be used to compare the degree of exfoliation of clay platelets in a polymer matrix. They concluded that well-exfoliated samples display a higher magnitude of $n$, whereas the absence of exfoliation results in $n$ values closer to zero. The fact that the value of $n$ was independent of clay concentration indicated the good exfoliation of clay up to 5 wt %, the highest concentration used in this study.

To further investigate the relationship between the shear-thinning exponent and the degree of exfoliation of organoclay in the paraffin wax matrix, samples containing 3% organoclay were melt-processed with both sonication with an ultrasonic processor and simple stirring with a magnetic stirring bar. Tensile tests for the samples carried out at 25°C showed modulus, yield strength, and percentage elongation at break values for the sonicated and stirred samples of 95 MPa, 0.8 MPa, and 41% and 68 MPa, 0.9 MPa, and 26%, respectively. Both samples demonstrated significant improvements over the pure paraffin wax, for which values of 61.4 MPa, 0.77 MPa, and 12%, respectively, were obtained. The greater stiffness and ductility for the sonicated sample were attributable to the higher degree of exfoliation. (It was shown previously that this preparation technique involving sonication provides for good dispersion and exfoliation of the organoclay in the wax matrix.[1,2]) Figure 7 compares η* of the stirred and sonicated composite samples. The differences were substantial. The sonicated mixture exhibited greater shear-thinning behavior than the stirred sample, and fits of the data with eq. (1) resulted in an $n$ value of −0.73 for the stirred sample, whereas the value for the sonicated sample ($n$ = −0.95) was significantly lower and close to −1. Also shown in the figure are the $G'$ and $G''$ values for the two samples. For the sonicated sample, $G'$ was greater than $G''$ for the entire frequency range tested, whereas this was the case only for low frequencies with the stirred

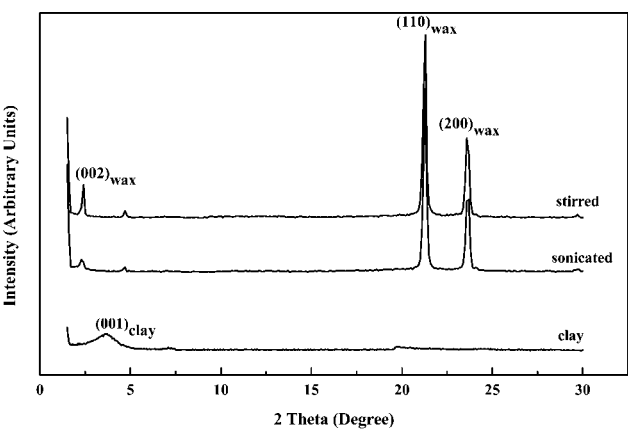


**Figure 8** XRD scans of wax nanocomposites prepared by stirring and sonication. A scan of the organoclay is also shown.

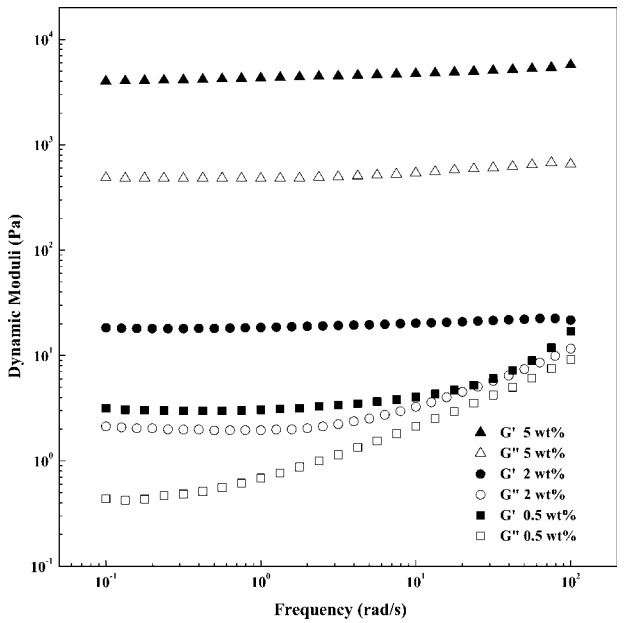


**Figure 9** Frequency dependence of dynamic moduli for wax nanocomposites containing various organoclay concentrations.

sample, which possessed a crossover point. The degree of exfoliation could not be confirmed for these samples with XRD. This is demonstrated in Figure 8, which shows the XRD scans for a 2θ range of 1.5–30°. The clay signal was absent in the scans for both the sonicated and stirred samples, even though the rheology data and our previous transmission electron microscopy results indicated a significant difference in the degree of exfoliation between the two samples. Thus, melt rheology may provide a useful technique for gauging the extent of exfoliation in the wax matrix, as was demonstrated for polymer matrices.[18]

A comparison of the frequency dependence of dynamic moduli for the nanocomposites measured at 70°C is shown in Figure 9. There was a monotonic increase in the dynamic moduli with increasing clay content. The nanocomposites all showed solidlike behavior at low frequencies. For the polymer nanocomposites, the low-frequency solidlike behavior was also observed and attributed to the physical jamming or percolation of the exfoliated/interacted clay network.[18,19] It was suggested that beyond a critical clay loading, the percolation threshold, the clay layers or tactoids are unable to rotate freely and, thus, prevent polymer chains from completely relaxing at low frequencies, which results in solidlike behaviors.[20] It has also been reported that exfoliated nanocomposites showed percolation behaviors at lower clay concentrations than intercalated nanocomposite systems.[21,22] The fact that the wax/clay nanocomposites exhibited a low-frequency solid behavior at clay concentrations as low as 0.5 wt % indicated a good exfoliation of the clay, as previously revealed by transmission electron microscopy.[1] With increasing clay content, the onset of frequency dependence was shifted to higher frequency values. The nanocomposites with lower clay loadings, 0.5 and 2 wt %, approached a crossover at high frequencies. When the clay concentration increased to 5 wt %, there was a solidlike response with nearly frequency-independent $G'$ and $G''$ values over all of the frequencies tested. The parallel $G'$ and $G''$ values with $G' > G''$ indicated a gel-like structure due to network formation from the well-dispersed silicate layers.[23,24] Gelling was indeed observed when we tried to remelt the wax nanocomposites at clay concentrations of greater than 3 wt %.

## CONCLUSIONS

Paraffin wax is an inexpensive petroleum byproduct that is soft, weak, and brittle and, thus, provides limited performance when exposed to even small loads in service. In addition, the wax often possesses rotator phases and softens near room temperature, which further limits its potential applications. It was shown in a previous work that clay addition significantly improved the mechanical properties of wax. In this study, the viscoelastic behavior of wax and its nanocomposites were examined over a broad temperature range, where accurate tensile measurements were not possible, which provided insight into the mechanism by which nanodisperse clays interact with an oligomeric matrix to produce uncommon enhancements in properties.

Dynamic mechanical analysis showed that the wax softened significantly and was more viscoelastic in its premelting region. The exfoliation of the organoclay increased $G'$ and decreased $G''$ in the low-temperature crystalline phase, while increasing both dynamic moduli in the mesophase region. This result means that the reinforcing effect of clay was retained in the mesophase region. The rheological study of molten nanocomposites showed a large increase in $\eta^*$ with clay addition. These nanocomposite samples demonstrated shear-thinning behavior, and $\eta^*$ versus $\omega$ data were fit well by a power-law function, where the shear-thinning constant was strongly related to the degree of exfoliation of clay, which was difficult to obtain via XRD. The molten samples demonstrated low-frequency solidlike behaviors; this was consistent with the good exfoliation obtained by ultrasonic processing. Melt rheology data for the nanocomposites provided important information on wax-layered silicate interactions and the structure–property relationship in nanocomposites and may also offer a useful gauge of the extent

to which an organoclay has been exfoliated and dispersed in wax matrices.

## References


1. Wang, J.; Severtson, S. J.; Stein, A. Adv Mater 2006, 18, 1585.
2. Wang, J.; Severtson, S. J.; Geil, P. H. Mater Sci Eng A 2007, 467, 172.
3. Rossetti, F.; Ranalli, G.; Faccenna, C. J Struct Geol 1999, 21, 2413.
4. Al-Fariss, T. F.; Jang, L. K.; Ozbelge, H. O.; Ghasem, N. M. J Pet Sci Eng 1993, 9, 139.
5. Tan, S. P.; Adidharma, H.; Towler, B. F.; Radosz, M. Ind Eng Chem Res 2006, 45, 2116.
6. McMillan, L. C.; Darvell, B. W. Dent Mater 2000, 16, 337.
7. Ungar, G. J Phys Chem 1983, 87, 689.
8. Ungar, G.; Masic, N. J Phys Chem 1985, 89, 1036.
9. Sirota, E. B.; King, H. E., Jr.; Singer, D. M.; Shao, H. H. J Chem Phys 1993, 98, 5809.
10. Sirota, E. B.; Singer, D. M. J Chem Phys 1994, 101, 10873.
11. Sirota, E. B.; King, H. E., Jr.; Shao, H. H.; Singer, D. M. J Phys Chem 1995, 99, 798.
12. Dorset, D. L. Acta Crystallogr B 1995, 51, 1021.
13. Craig, S. R.; Hastie, G. P.; Roberts, K. J.; Gerson, A. R.; Sherwood, J. N.; Tack, R. D. J Mater Chem 1998, 8, 859.
14. Craig, S. R.; Hastie, G. P.; Roberts, K. J.; Sherwood, J. N.; Tack, R. D.; Cernik, R. J. J Mater Chem 1999, 9, 2385.
15. Nowak, M. J.; Severtson, S. J. J Mater Sci 2001, 36, 14159.
16. Petitjean, D.; Schmitt, J. F.; Fiorani, J. M.; Laine, V.; Bouroukba, M.; Dirand, M.; Cunat, C. Fuel 2006, 85, 1323.
17. Wagener, R.; Reisinger, T. J. G. Polymer 2003, 44, 7513.
18. Ren, J.; Silva, A. S.; Krishnamoorti, R. Macromolecules 2000, 33, 3739.
19. Krishnamoorti, R.; Yurekli, K. Curr Opin Colloid Interface Sci 2001, 6, 464.
20. Gupta, R. K.; Pasanovic-Zujo, V.; Bhattacharya, S. N. J Non-Newtonian Fluid Mech 2005, 128, 116.
21. Krishnamoorti, R.; Giannelis, E. P. Macromolecules 1997, 30, 4097.
22. Hyun, Y. H.; Lim, S. T.; Choi, H. J.; Jhon, M. S. Macromolecules 2001, 34, 8084.
23. Zhong, Y.; Zhu, Z.; Wang, S. Q. Polymer 2005, 46, 3006.
24. Gisler, T.; Ball, R. C.; Weitz, D. A. Phys Rev Lett 1999, 82, 1064.